Charlotte, NC, USA), and the adjacent section was used for counter staining with hematoxylin and eosin (HE). The samples that were used for IMS were also stained with HE after analysis. Two authors (YI and HO) performed a microscopic examination of the HE stained glass slides of adjacent sections and those after IMS analysis. Breast cancer cells are identified from the findings that its cytoplasm is often abundant and eosinophilic and its nuclei may be regular, uniform or highly pleomorphic with prominent, often multiple, nucleoli, mitotic activity may be virtually absent or extensive [22]. Regions that were regarded as exhibiting insufficient pathological findings, whether benign or malignant, were excluded from the analysis.

IMS Analysis

A thin matrix layer was applied to the surface of the samples that were placed on ITO-coated glass slides by using a vapor deposition device (RK27-4069; Shimadzu Corporation, Kyoto, Japan) as previously reported [23].

MALDI-IMS was performed by using a MALDI-TOF/TOF-type instrument (Ultraflex II TOF/TOF; Bruker Daltonics). The machine was equipped with a 355-nm Nd: YAG laser that operated at a repetition rate of 200 Hz and was controlled by flexControl 2.4 software (Bruker Daltonics). The data were acquired in the range of m/z 400 (500 in 6 samples)-1000 by using step sizes of 90–130 μm for the samples in the positive ion mode. All of the spectra were acquired automatically using FlexImaging 2.1 software (Bruker Daltonics). The mass spectra were calibrated externally by using the bradykinin fragment 1–7 ($[M+H]^+$, m/z 757.39916), angiotensin II ($[M+H]^+$, m/z 1046.54180), and DHB ($[M+H]^+$, m/z 155.03000). Imaging reconstruction was performed using the FlexImaging 2.1 software (Bruker Daltonics).

Lipid Analysis

Twenty-nine specimens from 29 patients were provided for IMS analysis. After measurement and data reconstruction, we set regions of interest (ROIs) of approximately 500 μm×500 μm to obtain mean of signal intensities at the specified regions. We defined 'cancerous areas' as areas that contain cancer cells and cancer-free 'reference areas' as the rest of the measured areas on the sections, referring the HE staining of the section.

For the data analysis presented in Figures 3 and 5, we set 27 ROIs in the cancerous areas and 8 ROIs in the reference areas. All ROIs in cancerous and reference areas were carefully set by following the microscopic reexamination that was mentioned in the part of Sample preparation. Twenty-one cancerous ROIs were set on 21 sections, as each section contained 1 cancerous area (sample No. 1–9, 11, 13, 15–19, 21, 24, 25, 27, and 29). Two reference ROIs were set on 2 sections (sample No. 20 and 28). For the remaining 6 sections, we set both 1 cancerous ROI and 1 reference ROI on each section (sample No. 10, 12, 14, 22, 23, and 26).

For the data analysis for Figures S2 and S4, we used the data obtained from the measurement of 6 sections (sample No. 10, 12, 14, 22, 23, and 26). Three cancerous ROIs and 3 reference ROIs were set in each sample.

The signal intensity of each extracted m/z was calculated and exported by using FlexImaging 2.1 software. Previous reports [24,25] and a mass library (http://www.lipidmaps.org/data/structure/LMSDSearch.php) were used as references to make assignments for the molecular ions.

Most fatty acids that are produced in mammals usually have 16–18 carbons [26]. Based on this fact, the PCs whose number of carbons were 32, 34, or 36 and whose degree of unsaturation was 0 or 1 were defined as being representative PCs. Lysophosphatidylcholines (LPCs) that could be substrates for the generation of these PCs were considered to be representative LPCs.

The intensities of representative PCs and LPCs were recorded and compared between cancerous areas and reference areas. All of the statistical analyses were performed using Statcel2 software (OMS Ltd., Saitama, Japan). Welch's t-test (p value of <0.005) was used to perform statistical analysis on the peak intensity values of the cancerous and reference areas.

The ratios of MUFA-PCs to SFA-PCs and LPCs were compared between the cancerous areas and the reference areas. The ratio was calculated from the recorded intensities and analyzed by employing Welch's t-test (p value of <0.005) and using Statcel2 software.

A paired t-test (p value of <0.01) was used to perform statistical analysis of the intensities between the cancerous areas and reference areas in the supplemental analysis by considering the two areas on a single section as being a pair. Since the substantial sample size (the number of specimens provided to the analysis) in this comparison was small as six in each group, we used p value of 0.01 for threshold for examination of significance only in this analysis.

To investigate the relationship between clinical marker expression and the ratios of MUFA-PCs to SFA-PCs and LPCs in the cancerous areas, the ratio of MUFA-PCs to SFA-PCs and LPCs found by the difference of expression of ER, HER2, and Ki67 were calculated. Statistical analyses were performed by using Welch's t-test (p value of <0.005).

Immunohistochemical Staining

Immunohistochemical staining was performed to detect SCD1 expression. The formalin-fixed and paraffin-embedded specimens were sliced into 4–5 μm thick slices and mounted onto slide glass. The sections were de-paraffinized in xylene and rehydrated in a graded ethanol series. For antigen retrieval, the sections were heated in Tris-ethylenediaminetetraacetic acid buffer (pH 9.0) for 40 min. The sections were immersed in 3% H_2O_2/methanol for 5 min to quench endogenous peroxidase. Next, they were pre-incubated with 3% normal serum and then incubated with mouse monoclonal antibody against SCD1 (1:50; GeneTex, Irvine, CA, USA) overnight at 4°C. Following this, the sections were allowed to react with horseradish peroxidase-conjugated goat secondary antibody against mouse IgG (1:200, Vector Laboratories, Burlingame, CA, USA) for 2 h at 4°C. The sections were visualized by using a DAB substrate kit (Vector Laboratories), according to the manufacturer's instructions. Basal epithelial cells in the mammary gland were used as an inner negative control for SCD1 staining, by referring the previous report on SCD1 staining for prostate cancer tissues [27]. Apocrine cells in the skin were used as an inner positive control. Samples that were regarded as exhibiting insufficient staining or non-specific staining were excluded from the analysis. Three cancerous areas (sample No.16–18) were excluded for the analysis because of insufficient staining or non-specific staining. The remaining 24 cancerous areas and 8 reference areas were judged as areas that were stained appropriately. The expression levels for the positive cells were assessed by using Image J (NIH, Bethesda, MD, USA).

For the comprehensive analysis shown in Figure 4c, the expression levels of SCD1 were compared between 24 cancerous areas (sample No. 1–15, 19, 21–27, and 29; $n=24$) and 8 reference areas (sample No. 10, 12, 14, 20, 22, 23, 26, and 28; $n=8$). For sub-analysis in consideration of the ER status that is shown in Figure 6, cancerous lesions with positive ER (sample No. 2, 3, 6–9, 11, 13–15, 22–27, and 29; $n=17$) and those with

negative ER (sample No. 1, 4, 5, 10, 12, 19, and 21; n = 7) were analyzed. For sub-analysis considering HER2 status, cancerous lesions with negative HER2 (sample No. 2–7, 9, 10, 13–15, 21, 23–27, and 29; n = 18) and those with positive HER2 (sample No. 2, 8, 11, 12, 19, and 22; n = 8) were used. For sub-analysis considering Ki67, cancerous lesions with lower Ki67 (sample No. 2, 3, 6, 7, 9, 10, 13, 24, 25, 26, 27, and 29; n = 12) and those with higher Ki67 (sample No. 4, 5, 8, 11, 12, and 15; n = 6) were used. Welch's *t*-test (p value of <0.005) was used for the statistical analysis.

To examine the presence of bias in the distribution of SCD1 staining intensity and the MUFA-PC to SFA-PC ratio, the values from all samples that were correctly stained with SCD1 antibody were plotted two-dimensionally. A borderline was set to divide the plots and frequencies into quadrants that were subjected to Pearson's chi-square test (p value of <0.005) to examine if their distributions were different from the theoretical one. The presence of such borderlines on PCs with 32, 34, and 36 acyl carbons was examined by conducting the above procedure.

Results

Visualization by MALDI-IMS of PCs in Human Breast Cancer Tissues

We succeeded in visualizing some molecules by IMS. Figure 2 shows the images that were obtained on performing MALDI-IMS and an HE staining of the adjacent section. Since the samples that were used for IMS analysis were severely destroyed by laser irradiation, HE-stained images of adjacent sections were used for the identification of cancerous areas and are presented in the figures. The samples after IMS analysis were also stained by HE and ascertained by microscopic examination to closely resemble the adjacent tissue sections (Figure S1). The cancerous areas are indicated by broken red lines, and the stromal tissues that were around the ducts are circled with broken yellow lines in the HE-stained image (Figure 2a). Figure 2b and 2c depict typical images that were obtained by MALDI-IMS, which were used to visualize the maldistribution of PC(32:1)+K (Figure 2b) and PC(36:0)+K (Figure 2c) corresponding predominantly to the cancerous areas and the stromal tissues around the ducts, respectively. Figures 2d and 2e show an example of mass spectra obtained from the cancerous area (Figure 2d) and the stromal region (Figure 2e) of the section. The analyzed areas are indicated by blue and red squares on the HE-stained image of the adjacent section. The mass spectra of this sample showed that the signal of PC(32:1)+K at m/z 770.5 was predominantly detected in the cancerous areas, while the ion signal was substantially reduced in the stromal region. On the other hand, the signal of PC(36:0)+K at m/z 828.5 did not show higher accumulation in the cancerous area.

The Ratios of MUFA-PCs Compared to SFA-PCs were Significantly Higher in the Cancerous Areas

We asked whether there might be any molecules characteristically observed in the cancer cell regions. We defined reference areas as regions excluding cancerous areas that were identified pathologically. Then, the intensities of each molecule in the cancerous areas were compared to those in the reference areas. Differences in the ratios of MUFA-PCs to SFA-PCs were examined between the cancerous and reference areas as well.

The areas that are circled with broken red lines on the HE staining image show the cancerous areas (Figure 3a). The heat map images of each molecular ion (Figures 3b to 3g) and a comparison of the signal intensities of the cancerous areas and the reference areas by signal intensity plots (Figures 3h, j, k, and l) also showed high degrees of accumulation of PC(32:1)+K (Figures 3b and h; p = 1.58E-03), PC(34:1)+K (Figure 3d and j; p = 3.70E-06), PC(34:0)+K (Figures 3e and k; p = 5.80E-04), and PC(36:1)+K (Figures 3f and l; p = 1.30E-04) in the cancerous areas. The ratio of PC(36:1)+K to PC(36:0)+K (Figure 3p) was significantly higher in the cancerous areas than in the reference areas (p = 6.00E-04), while the ratio of PC(32:1)+K to PC(32:0) (Figure 3n) and the ratio of PC(34:1)+K to PC(34:0)+K (Figure 3o) did not show a statistical difference between these areas (p = 1.24E-02 and p = 0.690, respectively). Therefore, 4 out of 6 molecular species of MUFA-PC and SFA-PC showed higher intensities in the cancer cell areas, while none of the species showed lower intensity. Therefore, MUFA-PC with acyl chains of 36 carbons exhibited significantly high intensity compared to the SFA-PCs, and MUFA-PC with 32 acyl carbons showed the similar tendency although it was not accompanied by statistical significance.

In order to confirm how the lipids tended to be distributed by considering only the sections that had both cancer regions and reference regions, the ratios of MUFA-PCs to SFA-PCs were also compared between the cancerous areas and the reference areas by considering paring of the two areas on the same tissue sections. The number of samples that we could set 3 ROIs in the cancerous areas and 3 ROIs in the reference areas for each section was 6. The ratios of MUFA-PCs to SFA-PCs were calculated in the same way and analyzed by a paired *t*-test. Our results showed the same tendency as for the analysis using all of the sections; the ratios of PC(36:1)+K/PC(36:0)+K was significantly higher in the cancerous areas (p = 3.66E-03; Figure S2c).

High Expression of SCD1 Protein in Cancerous Areas

Past studies using cancer cell lines reported an important correlation between cancer cell proliferation and SCD1 [17,28,29]. We therefore examined whether the maldistribution of MUFA-PCs in the cancerous areas corresponded to SCD1 protein expression. Immunohistochemical staining revealed that SCD1 protein accumulated to a great degree in the cancerous areas (Figure 4a to c; p = 1.36E-07). We also examined whether the high ratio of MUFA-PC to SFA-PC coincided with high SCD1 expression by analyzing the frequencies of the quadrants in which the values of the subjects were plotted (Figure 4d, and Figure S3a and Sb). A biased distribution was confirmed by the chi-squared test in the case of PCs with 36 acyl carbons when a borderline was set so that the SCD1 intensity = 38 and the ratio = 3.5 (Figure 4d; p = 4.15E-03).

The Ratios of MUFA-PCs Compared to LPCs were Significantly Higher for the Cancerous Areas

The production of MUFA-PCs is also catalyzed by lysophosphatidylcholine acyltransferases (LPCATs), which transfer MUFAs to LPCs [30] (Figure 1). The amount of LPCs is considerably balanced through its use by LPCAT and its supply via the metabolization of PC by phospholypases A1 and A2 (plA1 and plA2) as well as phospholipid:diacylglycerol acyltransferases [31,32]. We next examined if this pool of LPCs showed a characteristic distribution in the cancer tissues in order to confirm that the accelerated synthesis was not due to the abundance of LPCs acting as substrates (Figure 5). A distribution of LPC(14:0)+K, LPC(16:0)+K and LPC(18:0)+K bias toward the cancerous areas was not observed (Figures 5c, e, g, i, k, and m; p = 0.221, p = 9.12E-02, and p = 0.128, respectively). To estimate the balance of PC synthesis and metabolization, we compared the ratios of MUFA-PC to LPC in the cancerous areas and the reference areas. The ratio of PC(36:1)+K to LPC(18:0)+K

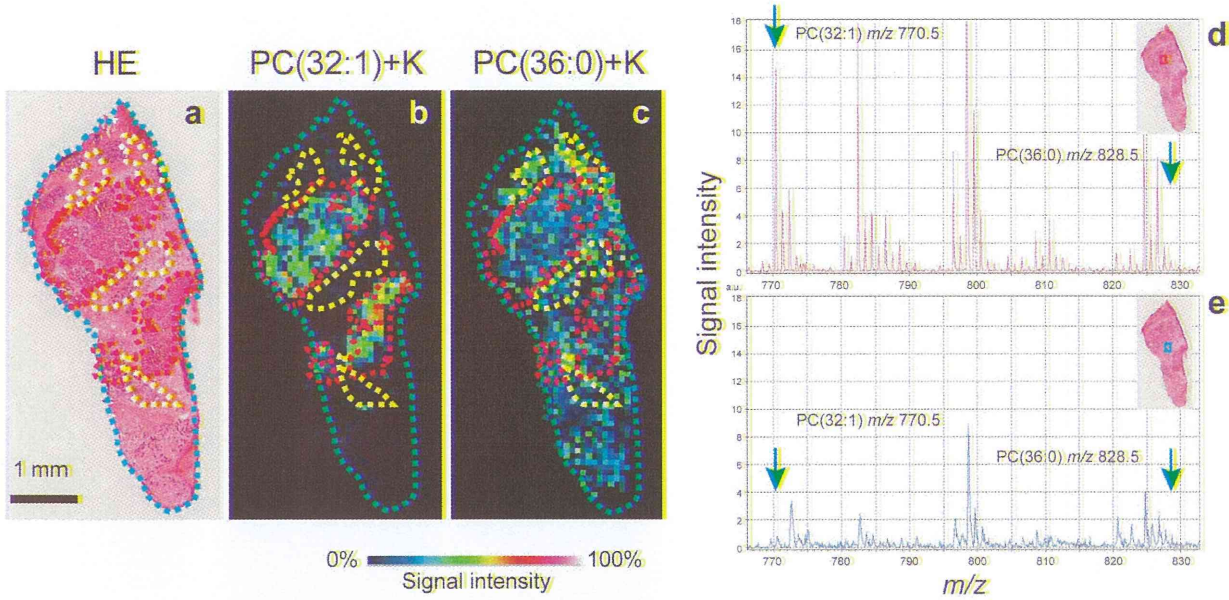

Figure 2. Different species of phosphatidylcholine were visualized on a breast cancer tissue specimen. (a) The areas that are circled with broken red lines in the adjacent hematoxylin and eosin (HE) stained images show cancerous areas and those that are circled with broken yellow lines show stromal tissue around the ducts. (b) A distribution image of PC(32:1)+K by MALDI-IMS shows the accumulation of PC(32:1)+K in the cancerous areas. (c) A distribution image of PC(36:0)+K shows the accumulation of PC(36:0)+K in the stromal tissue around the ducts. (d and e) Mass spectra obtained for a cancerous area shows different patterns from those of a reference area. The red and blue squares in the HE stained image in the inset shows the analytical points in a cancerous area and a reference area, respectively.
doi:10.1371/journal.pone.0061204.g002

(Figure 5p) was significantly higher in the cancerous areas than in the reference areas (p = 2.54E-03) and the ratios of PC(32:1)+K to LPC(14:0)+K and PC(34:1)+K to LPC(16:0)+K in the cancerous areas showed a tendency to be higher than those in the reference areas (Figure 5n and o; p = 8.50E-03 and p = 6.19E-02, respectively). Bias toward the synthesis of MUFA-PCs in the remodeling/degrading pathway in the cancerous areas was indicated.

The ratios of MUFA-PCs to LPCs in the cancerous area and the reference area located in the identical sections were also analyzed using the 6 tissue sections. The ratios of MUFA-PCs to LPCs were calculated and analyzed by using a paired *t*-test. Here as well, we obtained results that showed the same tendency as seen for the analysis using all of the sections: all of the ratios of MUFA-PCs to LPCs were significantly higher in the cancerous areas (Figures S4a to c; p = 1.37E-05 and p = 3.63E-03, and p = 9.79E-03, respectively).

The Ratios of MUFA-PCs Compared to SFA-PCs and to LPCs in the Cancerous Areas Observed through the Differences in Expressions of ER, HER2, and Ki67

Prognosis and survival rates for breast cancer vary greatly depending on the cancer subtype. ER negativity and HER2 positivity are known to be poor prognostic markers [33]. Ki67 is a nuclear protein that is present during all active phases of the cell cycle and is known to be a proliferation marker of many malignancies including breast cancer [34]. Therefore, we examined the SCD1 expression and the ratios of MUFA-PC compared to SFA and LPC considering the differences in expression of ER, HER2, and Ki67 (Figure 6). All of the cancerous lesions were divided into two groups: a less aggressive group that was ER positive, a group that was HER2 negative or showed low Ki67 expression, and a group that exhibited more aggressive ER negative, HER2 positive, or high Ki67 expression. Among the comparisons between the pairs of groups, only the comparison of the ratio of MUFA-PC [PC(34:1)] to SFA-PC [PC(34:0)] between the ER positive and negative specimens showed statistical significance: the ER positive lesions were higher than the ER negative lesions (Figure 6c; p = 2.50E-04). The other pairs including those for comparison in terms of SCD1 intensity did not show statistical differences while the lesions with negative HER2 showed a higher tendency ratio than did the HER2 positive lesions (Figure 6k; p = 5.86E-03).

Discussion

The visualization of molecules has contributed greatly to the characterization of clinical specimens derived from breast cancer patients. For example, the examination of protein expression of receptors such as HER2 and ER has been frequently used in classification [35,36], and fluorescent in situ hybridization is used to detect the amplification of oncogenes such as myc and HER2 [37]. On the other hand, lipids in clinical specimens have been investigated by nonspecific histochemistry using chemicals such as oil red [38]. This study firstly utilized MALDI-IMS to analyze clinical breast cancer specimens to visualize lipid discriminating acyl chain structures, quantitatively analyzed the region-specific signal intensities of multiple lipid molecules, and proposes a new methodology to clinically research breast cancer.

The system of PC synthesis that we focused on in this report was a remodeling pathway, which is one of two routes where PCs are synthesized: the de novo pathway (known as the Kennedy pathway) and the remodeling pathway (Land's pathway) [39]. In the remodeling pathway, MUFAs that are endogenously produced from SFAs through the influence of SCD1 are converted into

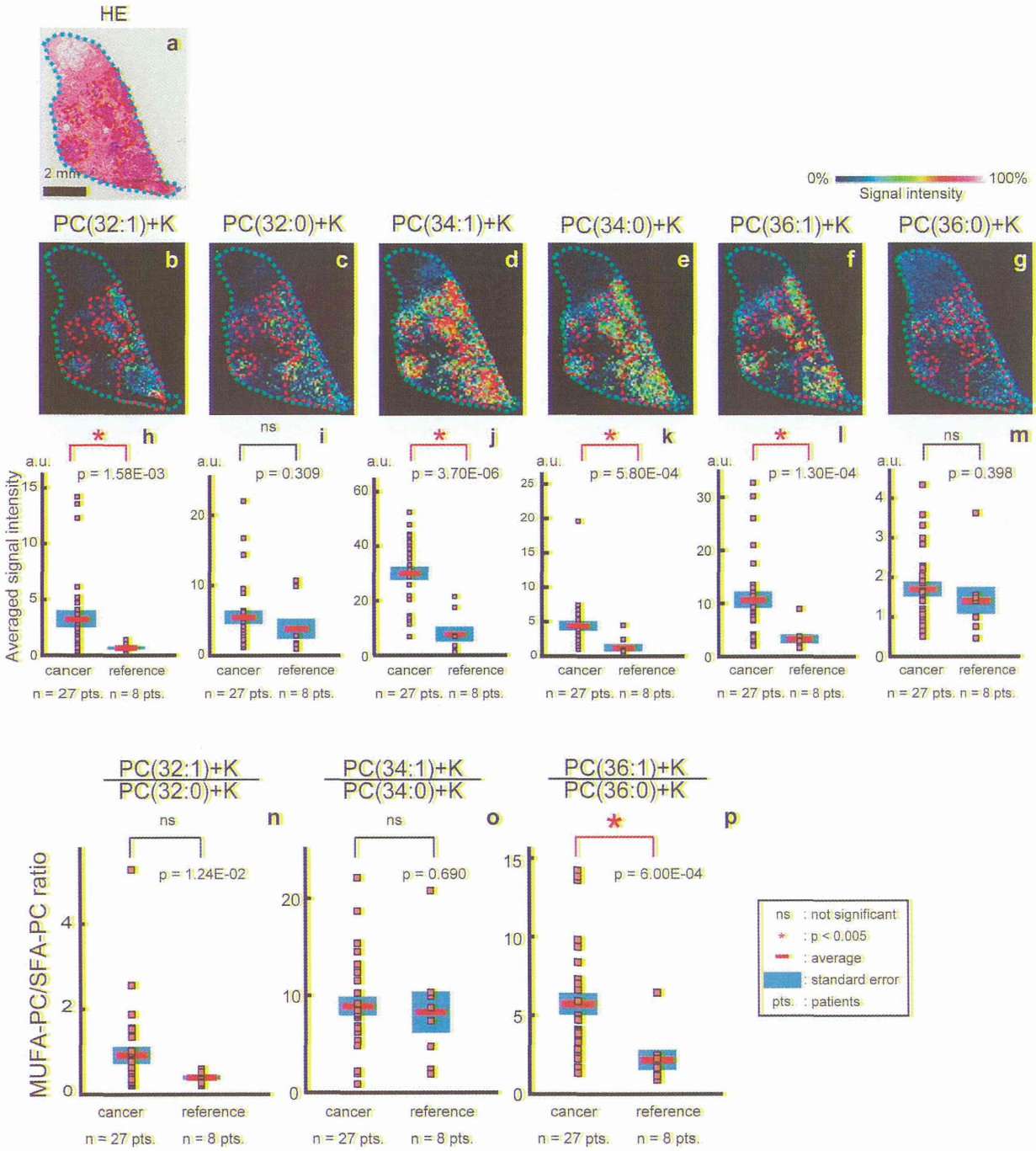

Figure 3. The amount of MUFA-PCs relative to SFA-PCs was significantly higher in cancerous areas. (a) The areas that are circled with broken red lines in the hematoxylin and eosin stained image show the cancerous areas. (b) A distribution image of PC(32:1)+K. (C) A distribution image of PC(32:0)+K. (d) A distribution image of PC(34:1)+K. (e) A distribution image of PC(34:0)+K. (f) A distribution image of PC(36:1)+K. (g) A distribution image of PC(36:0)+K. (h) Plot of the intensities of PC(32:1)+K. (i) Plot of the intensities of PC(32:0)+K. (j) Plot of the intensities of PC(34:1)+K. (k) Plot of the intensities of PC(34:0)+K. (l) Plot of the intensities of PC(36:1)+K. (m) Plot of the intensities of PC(36:0)+K. (n) Plot of the ratios of PC(32:1)+K to PC(32:0)+K. (o) Plot of the ratios of PC(34:1)+K to PC(34:0)+K. (p) Plot of the ratios of PC(36:1)+K to PC(36:0)+K.
doi:10.1371/journal.pone.0061204.g003

MUFA-PCs. Reports have shown varying levels of SCD1 expression in different tumor samples, including breast cancer [19,27], and higher SCD1 expression in breast cancer has been recently proposed as a poor prognostic marker [18]. To the best of our knowledge, this study is the first report showing that SCD1 is expressed in high levels in breast cancer cells in conjunction with

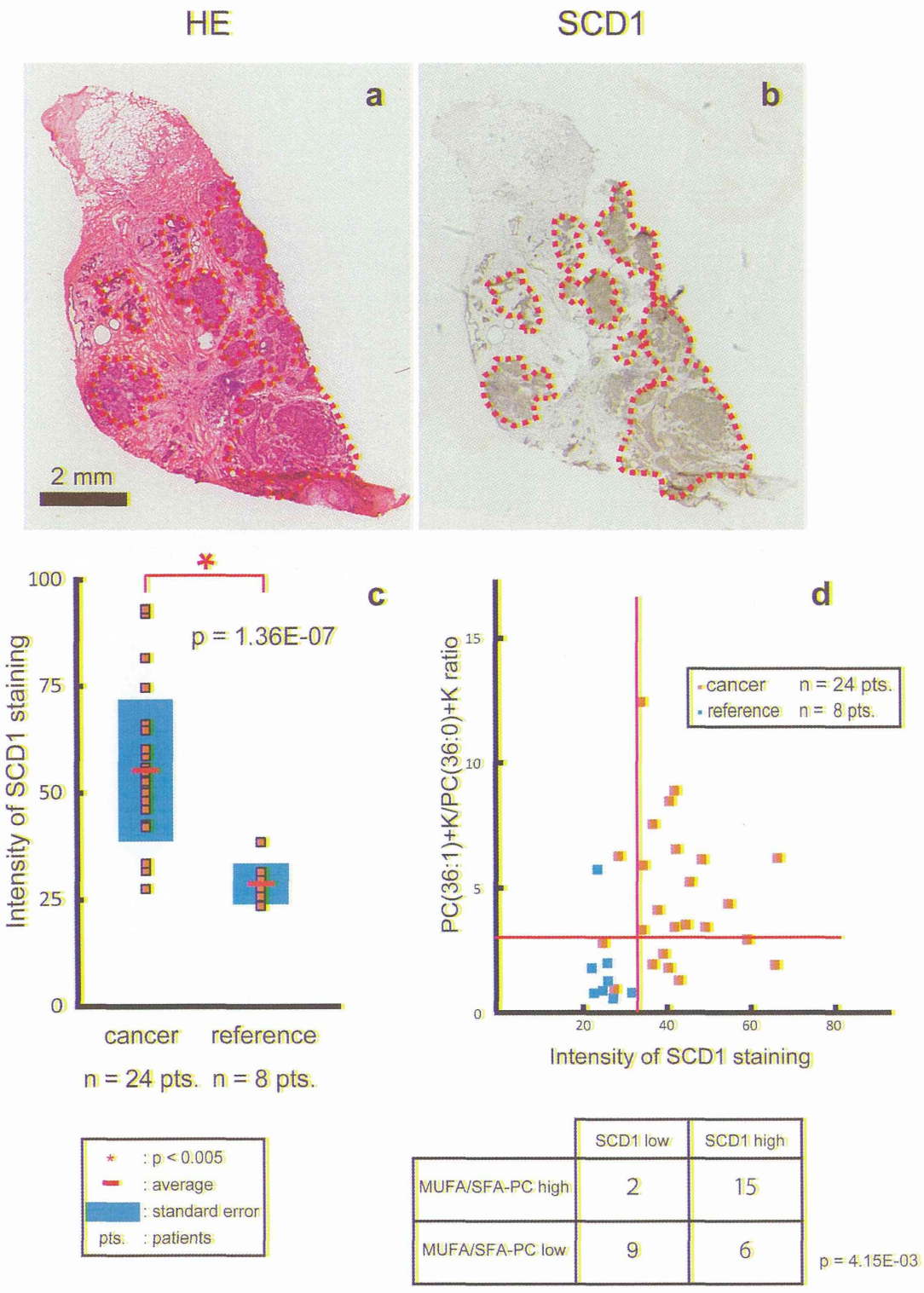

Figure 4. SCD1 protein was highly expressed in breast cancer tissues. (a) The areas that are circled with broken red lines in the hematoxylin and eosin stained image show cancerous areas. (b) Immunohistochemical staining for stearoyl-CoA desaturase-1 (SCD1) protein. (c) A plot of the intensities of SCD1 between the cancerous areas and the reference areas. (d) Values were plotted as SCD1 intensity on the x-axis and the MUFA-PCs/SFA-PCs ratio on the y-axis. The table shows the frequency of the subjects involved in each quadrant.
doi:10.1371/journal.pone.0061204.g004

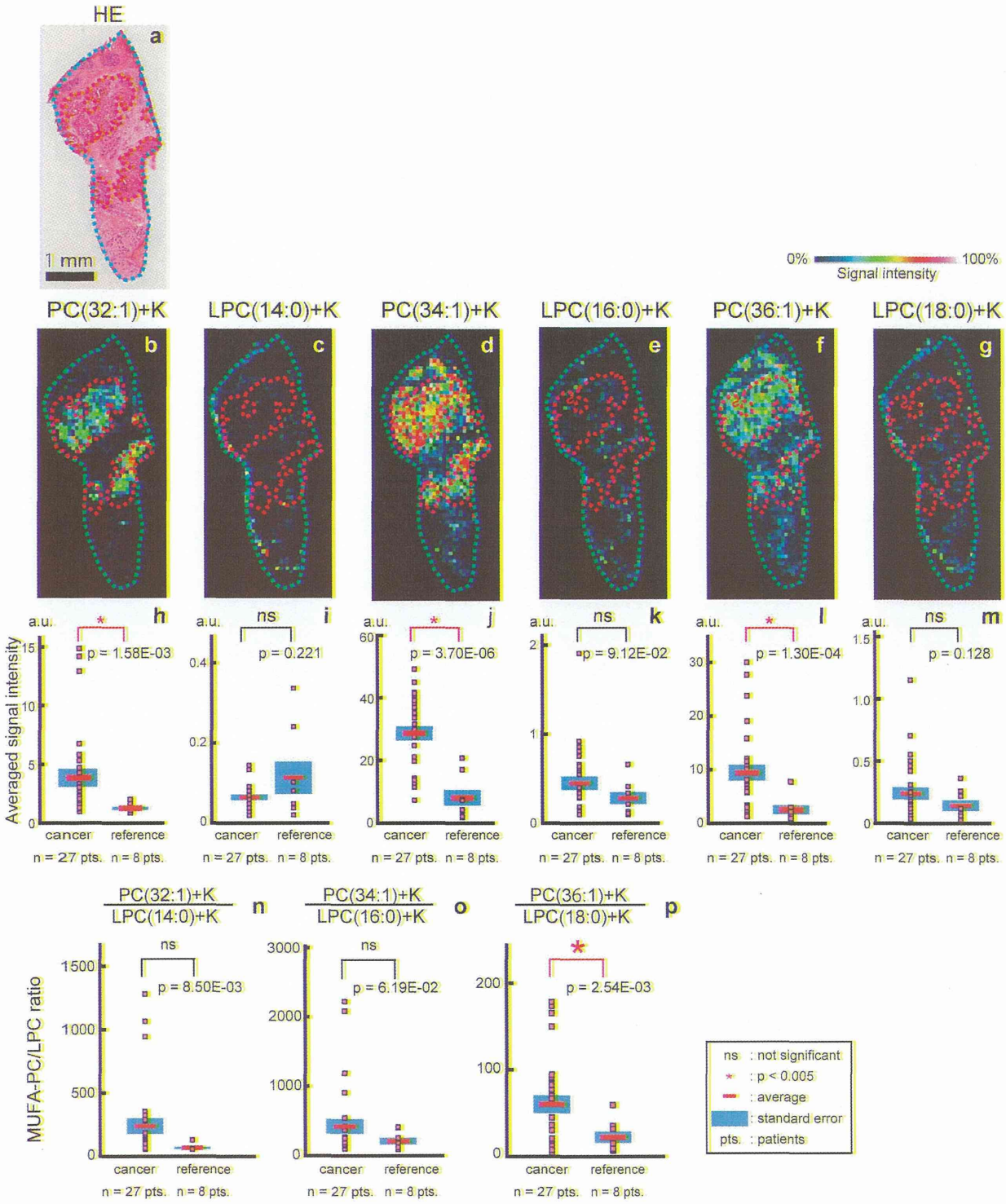

Figure 5. The ratios of MUFA-PCs to LPCs were significantly higher in cancerous areas than in reference areas. (a) The areas that are circled with red show the cancerous areas in the hematoxylin and eosin stained image. (b) A distribution image of PC(32:1)+K. (c) A distribution image of LPC(14:0)+K. (d) A distribution image of PC(34:1)+K. (e) A distribution image of LPC(16:0)+K. (f) A distribution image of PC(36:1)+K. (g) A distribution image of LPC(18:0)+K. (h) Plot of the intensities of PC(32:1)+K. (i) Plot of the intensities of LPC(14:0)+K. (j) Plot of the intensities of PC(34:1)+K. (k) Plot of the intensities of LPC(16:0)+K. (l) Plot of the intensities of PC(36:1)+K. (m) Plot of the intensities of LPC(18:0)+K in 35 ROIs. (n) Plot of the ratios of PC(32:1)+K to LPC(14:0)+K. (o) Plot of the ratios of PC(34:1)+K to LPC(16:0)+K. (p) Plot of the ratios of PC(36:1)+K to LPC(18:0)+K.
doi:10.1371/journal.pone.0061204.g005

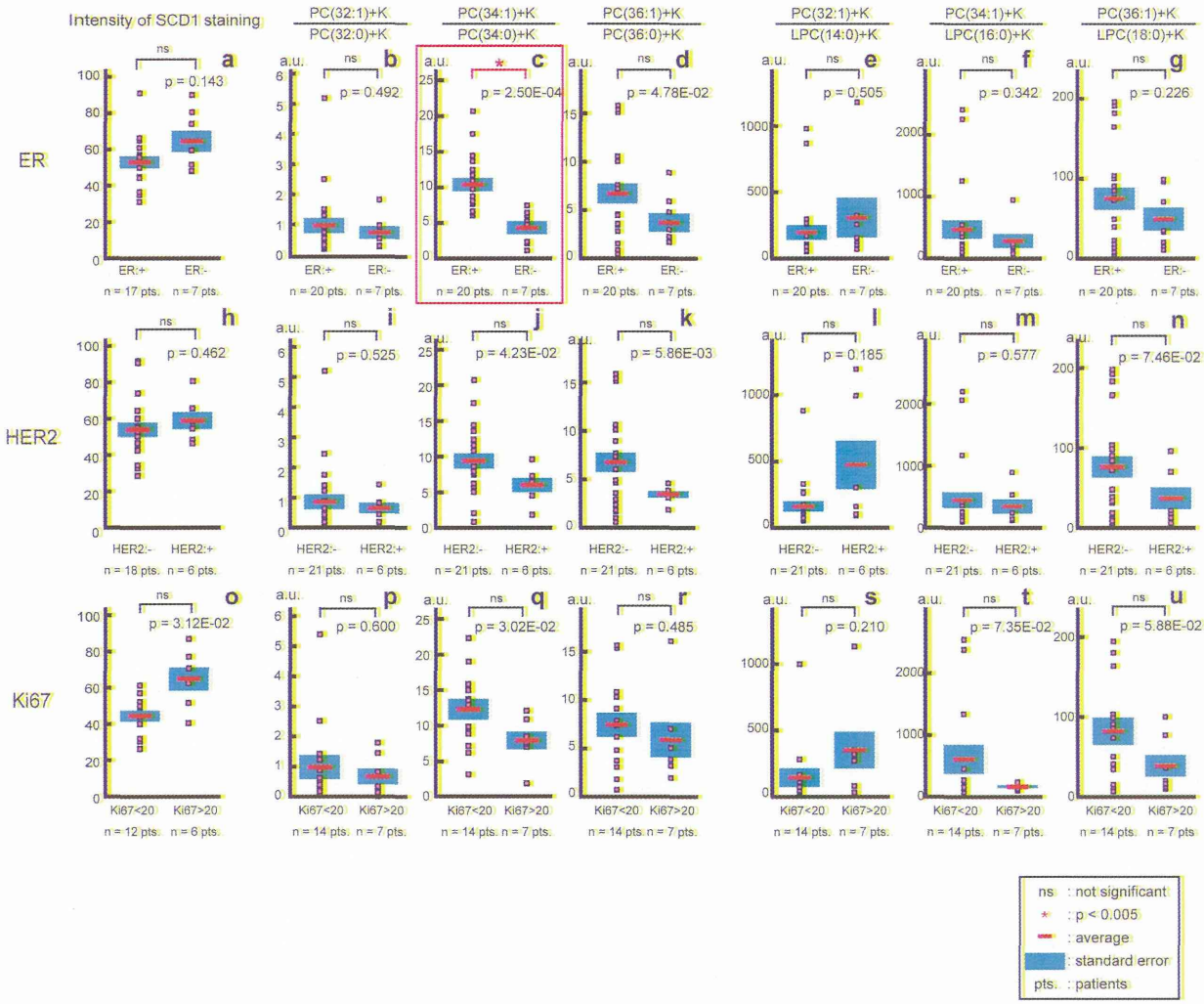

Figure 6. SCD1 expression and the ratios of MUFA-PCs to SFA-PCs and LPCs for differences in ER, HER2, and Ki67 expression. The intensities of SCD staining (a, h, o) and the ratios of MUFA-PC compared to SFA-PC (b–d, i–k, p–r) and LPC (e–g, l–n, s–u) were shown by the differences in ER (a–g), HER2 (h–n), and Ki67 (o–u). All of the cancer lesions were divided into two groups according to the differences in ER, HER2, and Ki67 expression and lesions with less aggressiveness are shown on the left side of each graph.
doi:10.1371/journal.pone.0061204.g006

a relatively high amount of MUFA-PCs. Among the 3 ratios of MUFA-PCs to SFA-PCs, only the ratio of PC(36:1) to PC(36:0) were found to be significantly related to the high SCD1 expression; this observation can be attributed to the SCD1 preferentially desaturating FA(18:0) over FA(16:0) [40]. The result that only the ratios of PC(36:1) to PC(36:0) in cancerous areas were higher might be explained by higher affinity of SCD1 to FA(18:0).

On the other hand, the result of a sub-analysis of the ratio of MUFA-PC [PC(34:1)] to SFA-PC [PC(34:0)] with respect to ER expression was not consistent with the SCD1 expression pattern: SCD1 expression did not show a significant difference between the ER positive groups and ER negative groups. This result could be explained by 2 possible reasons. First, there may be other factors that regulate the relative amount of MUFA-PCs. The LPCATs that catalyze the insertion of MUFAs into LPCs might be one of the candidates. [39,41]. We found from a microarray analysis that LPCAT3 is expressed at higher levels in ER positive tissues than in ER negative tissues [42,43], which is consistent with the correlation between ER status and the MUFA-PC/SFA-PC ratio that was observed in the present study. LPCAT4 is one LPCAT isoform that shows a higher specificity to FA(18:1) [44]. LPCAT4 may be acting as a regulating factor in this study as well, although no comparative studies on LPCAT4 expression between ER-positive and ER-negative breast cancer lesions have been reported. Second, a greater activity of the SCD1 enzyme in ER-positive cells than that in ER-negative cells could cause an excessive production of MUFA-PCs in these cells. As the endogenous mechanisms to regulate the enzymatic activity of SCD1 are poorly understood, further studies on the SCD1 activity and its regulatory mechanism might be warranted.

We alternatively defined tumor aggressiveness on the basis of immunohistochemical staining of pathological markers, ER negativity, HER2 positivity, and high Ki67 expression. Because exogenous HER2 overexpression induces upregulation of fatty acid synthase (FASN) in breast cancer cells, the pathway involving the HER2 receptor is generally considered to regulate lipogenic

enzymes [45]. The activation of lipid metabolism in tumor cell proliferation is widely accepted [2,3]; thus, the correlation of Ki67 expression level and PC compositions were expected. However, the ratios presented in Figure 6 did not show significant differences between high- and low-expression groups of HER2 and Ki67. We therefore could not prove the effect of the expression of these molecules on the acyl chains in PCs. Regarding the result that only the ratio of PC(34:1)/PC(34:0) showed significant differences between ER-positive and ER-negative groups, we propose the following mechanism. SCD1 predominantly converts FA(18:0) to FA(18:1) [40] and LPCATs combine FA(18:1) and LPC(16:0) [44], putatively the most abundant LPC, [46,47] to generate PC(34:1). Therefore, PC(34:1) might be preferentially affected by the alteration of expression and activity of the enzymes. However, further studies on this mechanism are warranted to confirm these statements that are based on propositions.

In this study, we analyzed the PCs of specific carbon chain lengths and saturation to characterize the specimens. Since polyunsaturated fatty acids have been argued to function in cancer hallmarks by maintaining and disrupting membrane microstructures and by tuning signal transductions [48,49], further studies involving PCs that are composed of fatty acids with longer chains and greater degrees of unsaturation might lead to a better understanding of the function of phospholipids in cancer pathogenesis.

Currently, MALDI-IMS as a technique is developing and is expected to have enough resolution to allow investigators to define and analyze smaller areas. If MALDI-IMS could be improved, it would be a useful tool for exploring the mechanisms of carcinogenesis and cancer metastasis. The analysis of cancer stem cells like treatment-resistant breast cancer cells that share small populations of thousands of cells in lesions [50] might be possible. A combination of improved MALDI-IMS and immunohistochemical staining might reveal a correlation between lipid composition and receptor expression, which has been scarcely reported [51]. MALDI-IMS has the potential to be a favorable tool to study breast cancer tissues with molecular heterogeneity [52]. We are attempting to improve the capabilities of MALDI-IMS by adopting new agents as a matrix [53], by using mass microscopes [54] and so on to perform these analyses in the near future.

Conclusions

IMS was used to successfully visualize molecular species of PCs and LPCs in human breast cancer tissue specimens. Some MUFA-PCs and SFA-PCs [PC(32:1), PC(34:1), PC(36:1), and PC(34:0)] were relatively localized in cancerous areas rather than the rest of the sections, while LPCs were equally distributed. Some ratios of MUFA-PCs to SFA-PCs or LPCs [PC(36:1)/PC(36:0) and PC(36:1)/LPC(18:0)] were higher in the cancerous areas than the references. The high expression of SCD1 in the cancerous areas was indicative that this enzyme partially mediates the production of MUFA-PCs that were observed in these areas. The analysis of the relative amount of MUFA-PC [PC(34:1) compared to PC(34:0)] through the differences in ER expression suggested the importance of other factors that regulate lipid composition.

Supporting Information

Figure S1 Samples after IMS analysis were severely damaged and closely resembled the adjacent tissue sections microscopically. (a) Adjacent tissue sections that were used for counter staining with hematoxylin and eosin (HE). (b) HE stained samples after IMS analysis.
(TIF)

Figure S2 Comparison of MUFA-PCs to SFA-PCs ratios between cancerous and reference areas on same tissue sections. (a) Plot of the ratios of PC(32:1)+K to PC(32:0)+K. (b) Plot of the ratios of PC(34:1)+K to PC(34:0)+K. (c) Plot of the ratios of PC(36:1)+K to PC(36:0)+K.
(TIFF)

Figure S3 Plot of SCD1 intensity and the MUFA-PCs/SFA-PCs ratio. The values from the subjects were plotted as SCD1 intensity on the x-axis and the MUFA-PCs/SFA-PCs ratio on the y-axis (a, b). A table shows the frequency of the subjects involved in each quadrant divided by the borderlines (a; p = 9.68E-03). The threshold with which bias in the frequencies in the quadrants were proven was not discovered for these molecules. The threshold and the frequency on PCs with 32 acyl carbons were presented since the examination showed relatively low p value.
(TIFF)

Figure S4 Comparison MUFA-PCs to LPCs ratios between cancerous and reference areas on same tissue sections. (a) Plot of the ratios of PC(32:1)+K to LPC(14:0)+K. (b) Plot of the ratios of PC(34:1)+K to LPC(16:0)+K. (c) Plot of the ratios of PC(36:1)+K to LPC(18:0)+K.
(TIFF)

Acknowledgments

We are grateful to the members of Division of Pathology of the Hamamatsu University School of Medicine Hospital for their kind assistance, Yayoi Kawabata and Naomi Suzuki in Department of Laboratory for Histological and Morphological Research, and Koji Ikegami, Noritaka Masaki, Kenji Ohata, Kensuke Goto, and Tsukasa Takahashi in the Department of Cell Biology and Anatomy of the Hamamatsu University School of Medicine for their useful advice.

Author Contributions

Conceived and designed the experiments: YI MW TN YM MS NS. Performed the experiments: YI MW TH TN YM HT TS. Analyzed the data: YI MW TH TN YM MS. Contributed reagents/materials/analysis tools: YI MW TH TN YM HT TS KK RM YH HO MS NS. Wrote the paper: YI MW TH KK MS.

References

1. Jemal A, Bray F, Center MM, Ferlay J, Ward E, et al. (2011) Global cancer statistics. CA Cancer J Clin 61: 69–90.
2. Menendez JA, Lupu R (2007) Fatty acid synthase and the lipogenic phenotype in cancer pathogenesis. Nat Rev Cancer 7: 763–777.
3. Blancato J, Singh B, Liu A, Liao DJ, Dickson RB (2004) Correlation of amplification and overexpression of the c-myc oncogene in high-grade breast cancer: FISH, in situ hybridisation and immunohistochemical analyses. Br J Cancer 90: 1612–1619.
4. Ekroos K, Ejsing CS, Bahr U, Karas M, Simons K, et al. (2003) Charting molecular composition of phosphatidylcholines by fatty acid scanning and ion trap MS3 fragmentation. J Lipid Res 44: 2181–2192.
5. Katz-Brull R, Seger D, Rivenson-Segal D, Rushkin E, Degani H (2002) Metabolic markers of breast cancer: enhanced choline metabolism and reduced choline-ether-phospholipid synthesis. Cancer Res 62: 1966–1970.
6. Podo F, Saradanelli F, Iorio E, Canese R, Carpinelli G, et al. (2007) Abnoramal Choline Phospholipid Metabolism in Breast and Ovary Cancer: Molecular Bases for Noninvasive Imgaging Approaches. Current Medical Imgaging Reviews 3: 123–137.
7. Glunde K, Jie C, Bhujwalla ZM (2004) Molecular causes of the aberrant choline phospholipid metabolism in breast cancer. Cancer Res 64: 4270–4276.

8. Bougnoux P, Chajes V, Lanson M, Hacene K, Body G, et al. (1992) Prognostic significance of tumor phosphatidylcholine stearic acid level in breast carcinoma. Breast Cancer Res Treat 20: 185–194.
9. Hilvo M, Denkert C, Lehtinen L, Muller B, Brockmoller S, et al. (2011) Novel Theranostic Opportunities Offered by Characterization of Altered Membrane Lipid Metabolism in Breast Cancer Progression. Cancer Research 71: 3236–3245.
10. Cornett DS, Reyzer ML, Chaurand P, Caprioli RM (2007) MALDI imaging mass spectrometry: molecular snapshots of biochemical systems. Nat Methods 4: 828–833.
11. Koizumi S, Hayasaka T, Goto-Inoue N, Doi K, Setou M, et al. (2012) Imaging mass spectrometry evaluation of the effects of various irrigation fluids in a rat model of postoperative cerebral edema. World Neurosurg 77: 153–159.
12. Chansela P, Goto-Inoue N, Zaima N, Hayasaka T, Sroyraya M, et al. (2012) Composition and localization of lipids in Penaeus merguiensis ovaries during the ovarian maturation cycle as revealed by imaging mass spectrometry. PLoS ONE 7: e33154.
13. Sugiura Y, Zaima N, Setou M, Ito S, Yao I (2012) Visualization of acetylcholine distribution in central nervous system tissue sections by tandem imaging mass spectrometry. Anal Bioanal Chem 403: 1851–1861.
14. Ntambi JM (1999) Regulation of stearoyl-CoA desaturase by polyunsaturated fatty acids and cholesterol. J Lipid Res 40: 1549–1558.
15. Scaglia N, Caviglia JM, Igal RA (2005) High stearoyl-CoA desaturase protein and activity levels in simian virus 40 transformed-human lung fibroblasts. Biochim Biophys Acta 1687: 141–151.
16. Mauvoisin D, Mounier C (2011) Hormonal and nutritional regulation of SCD1 gene expression. Biochimie 93: 78–86.
17. Luyimbazi D, Akcakanat A, McAuliffe PF, Zhang L, Singh G, et al. (2010) Rapamycin regulates stearoyl CoA desaturase 1 expression in breast cancer. Mol Cancer Ther 9: 2770–2784.
18. Holder AM, Gonzalez-Angulo AM, Chen H, Akcakanat A, Do KA, et al. (2013) High stearoyl-CoA desaturase 1 expression is associated with shorter survival in breast cancer patients. Breast Cancer Res Treat 137: 319–327.
19. Roongta UV, Pabalan JG, Wang X, Ryseck RP, Fargnoli J, et al. (2011) Cancer cell dependence on unsaturated fatty acids implicates stearoyl-CoA desaturase as a target for cancer therapy. Mol Cancer Res 9: 1551–1561.
20. Wolff AC, Hammond ME, Schwartz JN, Hagerty KL, Allred DC, et al. (2007) American Society of Clinical Oncology/College of American Pathologists guideline recommendations for human epidermal growth factor receptor 2 testing in breast cancer. Arch Pathol Lab Med 131: 18–43.
21. Nishimura R, Osako T, Okumura Y, Hayashi M, Toyozumi Y, et al. (2010) Ki-67 as a prognostic marker according to breast cancer subtype and a predictor of recurrence time in primary breast cancer. Exp Ther Med 1: 747–754.
22. Tavassoeli FA, Devilee P (2003) Pathology and Genetics of Tumours of the Breast and Female Genital Organs; Tavassoeli FA, Devilee P, editors: IARCPress.
23. Hayasaka T, Goto-Inoue N, Ushijima M, Yao I, Yuba-Kubo A, et al. (2011) Development of imaging mass spectrometry (IMS) dataset extractor software, IMS convolution. Anal Bioanal Chem 401: 183–193.
24. Hayasaka T, Goto-Inoue N, Zaima N, Kimura Y, Setou M (2009) Organ-specific distributions of lysophosphatidylcholine and triacylglycerol in mouse embryo. Lipids 44: 837–848.
25. Shrivas K, Hayasaka T, Goto-Inoue N, Sugiura Y, Zaima N, et al. (2010) Ionic Matrix for Enhanced MALDI Imaging Mass Spectrometry for Identification of Phospholipids in Mouse Liver and Cerebellum Tissue Sections. Anal Chem 82: 8800–8806.
26. Arita M (2012) Biological importance of fatty acids: from quantity and quality. Experimental Medicine 30: 406–411.
27. Moore S, Knudsen B, True LD, Hawley S, Etzioni R, et al. (2005) Loss of stearoyl-CoA desaturase expression is a frequent event in prostate carcinoma. International Journal of Cancer 114: 563–571.
28. Hilvo M, Denkert C, Lehtinen L, Muller B, Brockmoller S, et al. (2011) Novel theranostic opportunities offered by characterization of altered membrane lipid metabolism in breast cancer progression. Cancer Res 71: 3236–3245.
29. Scaglia N, Chisholm JW, Igal RA (2009) Inhibition of StearoylCoA Desaturase-1 Inactivates Acetyl-CoA Carboxylase and Impairs Proliferation in Cancer Cells: Role of AMPK. PLoS ONE 4: e6812.
30. Hishikawa D, Shindou H, Kobayashi S, Nakanishi H, Taguchi R, et al. (2008) Discovery of a lysophospholipid acyltransferase family essential for membrane asymmetry and diversity. Proc Natl Acad Sci U S A 105: 2830–2835.
31. Iorio E, Ricci A, Bagnoli M, Pisanu ME, Castellano G, et al. (2010) Activation of phosphatidylcholine cycle enzymes in human epithelial ovarian cancer cells. Cancer Res 70: 2126–2135.
32. Chen JE, Smith AG (2012) A look at diacylglycerol acyltransferases (DGATs) in algae. J Biotechnol 162: 28–39.
33. Sorlie T, Tibshirani R, Parker J, Hastie T, Marron JS, et al. (2003) Repeated observation of breast tumor subtypes in independent gene expression data sets. Proc Natl Acad Sci U S A 100: 8418–8423.
34. Scholzen T, Gerdes J (2000) The Ki-67 protein: from the known and the unknown. J Cell Physiol 182: 311–322.
35. Wolff AC, Hammond ME, Schwartz JN, Hagerty KL, Allred DC, et al. (2007) American Society of Clinical Oncology/College of American Pathologists guideline recommendations for human epidermal growth factor receptor 2 testing in breast cancer. J Clin Oncol 25: 118–145.
36. Hammond ME, Hayes DF, Dowsett M, Allred DC, Hagerty KL, et al. (2010) American Society of Clinical Oncology/College Of American Pathologists guideline recommendations for immunohistochemical testing of estrogen and progesterone receptors in breast cancer. J Clin Oncol 28: 2784–2795.
37. Kallioniemi OP, Kallioniemi A, Kurisu W, Thor A, Chen LC, et al. (1992) ERBB2 amplification in breast cancer analyzed by fluorescence in situ hybridization. Proc Natl Acad Sci U S A 89: 5321–5325.
38. Espinosa de los Monteros A, Hellmen E, Ramirez GA, Herraez P, Rodriguez F, et al. (2003) Lipid-rich carcinomas of the mammary gland in seven dogs: clinicopathologic and immunohistochemical features. Vet Pathol 40: 718–723.
39. Shindou H, Hishikawa D, Harayama T, Yuki K, Shimizu T (2009) Recent progress on acyl CoA: lysophospholipid acyltransferase research. J Lipid Res 50 Suppl: S46–51.
40. Miyazaki M, Kim HJ, Man WC, Ntambi JM (2001) Oleoyl-CoA is the major de novo product of stearoyl-CoA desaturase 1 gene isoform and substrate for the biosynthesis of the Harderian gland 1-alkyl-2,3-diacylglycerol. J Biol Chem 276: 39455–39461.
41. Zhao Y, Chen YQ, Bonacci TM, Bredt DS, Li S, et al. (2008) Identification and characterization of a major liver lysophosphatidylcholine acyltransferase. J Biol Chem 283: 8258–8265.
42. EMBL-EBI Available: http://www.ebi.ac.uk/gxa/experiment/E-TABM-276/ENSG00000111684/test_result Accessed November 27 2012.
43. Cheng AS, Culhane AC, Chan MW, Venkataramu CR, Ehrich M, et al. (2008) Epithelial progeny of estrogen-exposed breast progenitor cells display a cancer-like methylome. Cancer Res 68: 1786–1796.
44. Hishikawa D, Shindou H, Kobayashi S, Nakanishi H, Taguchi R, et al. (2008) Discovery of a lysophospholipid acyltransferase family essential for membrane asymmetry and diversity. Proceedings of the National Academy of Sciences 105: 2830–2835.
45. Yoon S, Lee MY, Park SW, Moon JS, Koh YK, et al. (2007) Up-regulation of acetyl-CoA carboxylase alpha and fatty acid synthase by human epidermal growth factor receptor 2 at the translational level in breast cancer cells. J Biol Chem 282: 26122–26131.
46. Sutphen R, Xu Y, Wilbanks GD, Fiorica J, Grendys EC, Jr., et al. (2004) Lysophospholipids are potential biomarkers of ovarian cancer. Cancer Epidemiol Biomarkers Prev 13: 1185–1191.
47. Chughtai K, Jiang L, Greenwood TR, Glunde K, Heeren RM (2013) Mass spectrometry images acylcarnitines, phosphatidylcholines, and sphingomyelin in MDA-MB-231 breast tumor models. J Lipid Res 54: 333–344.
48. Rockett BD, Franklin A, Harris M, Teague H, Rockett A, et al. (2011) Membrane raft organization is more sensitive to disruption by (n-3) PUFA than nonraft organization in EL4 and B cells. J Nutr 141: 1041–1048.
49. Chenais B, Blanckaert V (2012) The janus face of lipids in human breast cancer: how polyunsaturated Fatty acids affect tumor cell hallmarks. Int J Breast Cancer 2012: 712536.
50. Al-Ejeh F, Smart CE, Morrison BJ, Chenevix-Trench G, Lopez JA, et al. (2011) Breast cancer stem cells: treatment resistance and therapeutic opportunities. Carcinogenesis 32: 650–658.
51. Opekarova M, Tanner W (2003) Specific lipid requirements of membrane proteins–a putative bottleneck in heterologous expression. Biochim Biophys Acta 1610: 11–22.
52. Stingl J, Caldas C (2007) Molecular heterogeneity of breast carcinomas and the cancer stem cell hypothesis. Nat Rev Cancer 7: 791–799.
53. Shrivas K, Hayasaka T, Sugiura Y, Setou M (2011) Method for simultaneous imaging of endogenous low molecular weight metabolites in mouse brain using TiO2 nanoparticles in nanoparticle-assisted laser desorption/ionization-imaging mass spectrometry. Anal Chem 83: 7283–7289.
54. Waki ML, Onoue K, Takahashi T, Goto K, Saito Y, et al. (2011) Investigation by imaging mass spectrometry of biomarker candidates for aging in the hair cortex. PLoS ONE 6: e26721.

Research Article

EASL EUROPEAN ASSOCIATION FOR THE STUDY OF THE LIVER | JOURNAL OF HEPATOLOGY

Lysophosphatidylcholine acyltransferase 1 altered phospholipid composition and regulated hepatoma progression

Yoshifumi Morita[1,2], Takanori Sakaguchi[1], Koji Ikegami[2], Naoko Goto-Inoue[2], Takahiro Hayasaka[2], Vu Thi Hang[2], Hiroki Tanaka[1], Takashi Harada[1], Yasushi Shibasaki[1], Atsushi Suzuki[1], Kazuhiko Fukumoto[1], Keisuke Inaba[1], Makoto Murakami[3], Mitsutoshi Setou[2,*], Hiroyuki Konno[1]

[1]*Second Department of Surgery, Hamamatsu University School of Medicine, Japan;* [2]*Department of Cell Biology and Anatomy, Hamamatsu University School of Medicine, Japan;* [3]*Lipid Metabolism Project, Department of Advanced Science for Biomolecules, Tokyo Metropolitan Institute of Medical Science, Japan*

Background & Aims: Several lipid synthesis pathways play important roles in the development and progression of hepatocellular carcinoma (HCC), although the precise molecular mechanisms remain to be elucidated. Here, we show the relationship between HCC progression and alteration of phospholipid composition regulated by lysophosphatidylcholine acyltransferase (LPCAT).

Methods: Molecular lipidomic screening was performed by imaging mass spectrometry (IMS) in 37 resected HCC specimens. RT-PCR and Western blotting were carried out to examine the mRNA and protein levels of LPCATs, which catalyze the conversion of lysophosphatidylcholine (LPC) into phosphatidylcholine (PC) and have substrate specificity for some kinds of fatty acids. We examined the effect of LPCAT1 overexpression or knockdown on cell proliferation, migration, and invasion in HCC cell lines.

Results: IMS revealed the increase of PC species with palmitoleic acid or oleic acid at the *sn-2*-position and the reduction of LPC with palmitic acid at the *sn-1*-position in HCC tissues. mRNA and protein of LPCAT1, responsible for LPC to PC conversion, were more abundant in HCCs than in the surrounding parenchyma. In cell line experiments, LPCAT1 overexpression enriched PCs observed in IMS and promoted cell proliferation, migration, and invasion. LPCAT1 knockdown did *viceversa*.

Conclusions: Enrichment or depletion of some specific PCs, was found in HCC by IMS. Alteration of phospholipid composition in HCC would affect tumor character. LPCAT1 modulates phospholipid composition to create favorable conditions to HCC cells. LPCAT1 is a potent target molecule to inhibit HCC progression.

Keywords: Cancer lipidomics; Imaging mass spectrometry; LPCAT1; Hepatocellular carcinoma.

Received 4 May 2012; received in revised form 8 February 2013; accepted 18 February 2013

* Corresponding author. Address: Department of Cell Biology and Anatomy, Hamamatsu University School of Medicine, 1-20-1 Handayama, Higashi-ku, Hamamatsu 431-3192, Japan. Tel./fax: +81 53 435 2292.

E-mail address: setou@hama-med.ac.jp (M. Setou).

Abbreviations: HCC, hepatocellular carcinoma; NAFLD, non-alcoholic fatty liver disease; IMS, imaging mass spectrometry; MALDI, matrix-assisted laser desorption/ionization; LPCAT, lysophosphatidylcholine acyltransferase; PCA, principal component analysis; $cPLA_2\alpha$, cytosolic phospholipase $A_2\alpha$; $iPLA_2\beta$, Ca^{2+}-independent phospholipase $A_2\beta$; LPC, lysophosphatidylcholine; PC, phosphatidylcholine; DPPC, dipalmitoyl phosphatidylcholine; PAF, platelet activating factor.

Introduction

Hepatocellular carcinoma (HCC) is the seventh most frequently diagnosed cancer and the fourth most frequent cause of cancer-related death in the world [1]. The frequency of HCC has increased in the United States and in European and Asian countries [2]. In addition to HBV, HCV, alcohol, and aflatoxin, non-alcoholic fatty liver disease (NAFLD) has drawn increasing attention as a risk factor of HCC. NAFLD is the most common form of chronic liver disease in developed countries. Alteration of the lipogenic pathway plays an important role in the pathogenesis of NAFLD and also in HCC carcinogenesis and its progression [3].

In recent years, imaging mass spectrometry (IMS) using matrix-assisted laser desorption/ionization (MALDI) has emerged and developed dramatically in the field of proteomics and metabolomics [4,5]. MALDI-IMS can clarify the distribution of lipid molecules, directly from heterogeneous tissue samples, by determining the differences in the mass-to-charge ratios (m/z). Furthermore, tandem mass spectrometry (MS/MS analysis), which generates the fragment ion spectrum by spraying additional collision gas, enables the identification of the molecules in tissues by providing detailed information on their structures. IMS has been used to classify tumor grade or to investigate new biomarkers in cancer proteomics [6,7]. At present, there are only limited reports on molecular proteomics of HCC using IMS [8,9].

In this study, we performed IMS using HCC tissue samples as molecular lipidomic screening and revealed the alteration of phospholipid composition caused by overexpressed LPCAT1. We further investigated the role of LPCAT1 in HCC progression and

Please cite this article in press as: Morita Y et al. Lysophosphatidylcholine acyltransferase 1 altered phospholipid composition and regulated hepatoma progression. J Hepatol (2013), http://dx.doi.org/10.1016/j.jhep.2013.02.030